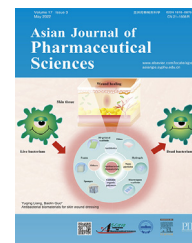Available online at www.sciencedirect.com

ScienceDirect

journal homepage: www.elsevier.com/locate/AJPS

Original Research Paper

Salvianolic acid B dry powder inhaler for the treatment of idiopathic pulmonary fibrosis

Peng Lu [a,b,c,e,#], *Jiawei Li* [d,#], *Chuanxin Liu* [f], *Jian Yang* [a,c], *Hui Peng* [a,b,c], *Zhifeng Xue* [a,c], *Zhidong Liu* [a,b,c,*]

[a] *State Key Laboratory of Component-Based Chinese Medicine, Tianjin University of Traditional Chinese Medicine, Tianjin 301617, China*
[b] *Engineering Research Center of Modern Chinese Medicine Discovery and Preparation Technique, Ministry of Education, Tianjin 301617, China*
[c] *Haihe Laboratory of Modern Chinese Medicine, Tianjin 301617, China*
[d] *College of Chinese Medicine, Tianjin University of Traditional Chinese Medicine, Tianjin 301617, China*
[e] *Department of Pharmacy, Suzhou TCM Hospital Affiliated to Nanjing University of Chinese Medicine, Suzhou, Jiangsu 215009, China*
[f] *Endocrine and Metabolic Disease Center, The First Affiliated Hospital, and College of Clinical Medicine of Henan University of Science and Technology, Medical Key Laboratory of Hereditary Rare Diseases of Henan, Luoyang Sub-center of National Clinical Research Center for Metabolic Diseases, Luoyang, Henan 471003, China.*

ARTICLE INFO

ABSTRACT

Idiopathic pulmonary fibrosis (IPF) is a serious and fatal pulmonary inflammatory disease with an increasing incidence worldwide. The drugs nintedanib and pirfenidone, are listed as conditionally recommended drugs in the "Evidence-Based Guidelines for the Diagnosis and Treatment of Idiopathic Pulmonary Fibrosis". However, these two drugs have many adverse reactions in clinical application. Salvianolic acid B (Sal B), a water-soluble component of Salvia miltiorrhiza, could alleviate bleomycin-induced peroxidative stress damage, and prevent or delay the onset of IPF by regulating inflammatory factors and fibrotic cytokines during the disease's progression. However, Sal B is poorly absorbed orally, and patient compliance is poor when administered intravenously. Therefore, there is an urgent need to find a new non-injection route of drug delivery. In this study, Sal B was used as model drug and L-leucine (LL) as excipient to prepare Sal B dry powder inhaler (Sal B-DPI) by spray drying method. Modern preparation evaluation methods were used to assess the quality of Sal B-DPI. Sal B-DPI is promising for the treatment of IPF, according to studies on pulmonary irritation evaluation, *in vivo* and *in vitro* pharmacodynamics, metabolomics, pharmacokinetics, and lung tissue distribution.

---

* Corresponding authors.
  E-mail address: liuzhidong@tjutcm.edu.cn (Z.D. Liu).
# These authors contributed equally to this work.
  Peer review under responsibility of Shenyang Pharmaceutical University.

1. Introduction

Idiopathic Pulmonary Fibrosis (IPF) is a common alveolar disease in which normal lung tissue is replaced by excessive interstitial cells and extracellular matrix, resulting in the destruction of alveolar structures, the gradual densification of the alveolar region, and ultimately respiratory failure and even death [1–6]. The age of onset of IPF is mostly between 50 and 70 years old. With the aging of the population, the incidence of IPF worldwide is increasing year by year. According to the statistics of the World IPF Joint Association, there are about 3.2 million people suffering from IPF and 1.22 million new cases every year [6]. Studies have shown that environmental factors (inhalation of dust, metal powder and wood chips in the air), viral infection (influenza virus, hepatitis C virus, etc.), gastroesophageal reflux and smoking are the main potential pathogenic factors for IPF. Since December 2019, there has been an outbreak of Coronavirus disease 2019 (COVID-19) in Wuhan, Hubei Province. Patients with severe COVID-19 may have left a certain degree of changes in lung damage repair for a period of time, such as the IPF [7–9]. The autopsy results of the first case of COVID-19 showed severe pulmonary fibrosis, although the pulmonary fibrosis and parenchymal lesions were not as severe as those caused by the SARS virus [9]. Current studies have shown that the pathological changes were due to the combined effects of oxidative stress, inflammatory response and fibrosis [2–5].

The commonly used drugs for clinical treatment of IPF mainly include tyrosine kinase inhibitors, cytokine inhibitors, glucocorticoids, collagen synthesis inhibitors, immunosuppressants, phosphodiesterase inhibitors, anticoagulants, endothelin antagonists and antioxidants [2]. There was no definitive and effective treatment other than lung transplantation, and without lung transplantation, the mortality rate for IPF patients was 50% at 3 years and 80% at 5 years [2–5], respectively. However, lung transplantation had problems such as scarcity of lung donor, high risk and cost. Currently, in the evidence-based guidelines for the diagnosis and treatment of IPF, only nitanib, a tyrosine kinase inhibitor, and pirfenidone, a cytokine inhibitor, are listed as conditional recommended drugs [10]. However, the above two drugs have large clinical dosage, high treatment cost, and are prone to drug resistance and more adverse reactions (diarrhea, rash, insomnia and dizziness, etc.) [11–12]. Therefore, it is of great economic value and social significance to continue to search for safe and effective drugs for the treatment of IPF.

Traditional Chinese medicine (TCM) is an integral part of modern medicine. It is also an important resource of natural medicines and plays a broader role in the treatment of human diseases [13]. In recent years, there have been many studies on TCM prevention or treatment of IPF [13–14]. Salvia miltiorrhiza is one of herbal medicines commonly used in the treatment of IPF [15]. Its water-soluble component, salvianolic acid, is the main active component to promote blood circulation and remove blood stasis. It not only has a protective effect on the cardiovascular system, but also plays an important role in the treatment of pulmonary diseases such as IPF and chronic obstructive pulmonary disease [14]. Salvianolic acid B (Sal B), the main component of salvianolic acid, could relieve bleomycin-induced peroxide-stress injury and regulate Tumor necrosis factor-α (TNF-α) and other inflammatory cytokines and fibrosis related cytokines to prevent or treat pulmonary fibrosis [16–17]. However, Sal B is poorly absorbed orally and rapidly eliminated *in vivo*. It has obvious liver first-pass effect and hepatointestinal circulation, and its absolute bioavailability is between 0.02% and 5.56% [18–20]. The way of injection administration can make the drugs directly enter the body to play its role, and the therapeutic effect is very good. However, it needs long-term and frequent intravenous administration to maintain the therapeutic effect, which leads to poor patient compliance due to the inconvenience of the way of use. Therefore, there is an urgent need to find a new non-injection route of drug delivery.

Pulmonary delivery as a non-injectable drug delivery route can target drug delivery to the lungs, avoiding low systemic toxicity due to intestinal absorption and liver metabolism [21]. The lungs have a large drug absorption surface area (about 100–140m^2), relatively high blood flow, low enzyme activity and thin epithelial cells, which have unique advantages for the treatment of lung diseases [22]. Compared with nebulizer (NEB) and metered dose inhaler (MDI), dry powder inhaler(DPI) has the advantages of good drug stability, convenient use and carrying, no need for ejectors, larger drug delivery doses, and good patient compliance [23]. At present, the preparation methods of DPI mainly include grinding method, spray freeze drying method, spray drying method, airflow crushing method and supercritical fluid technology [24]. DPI mainly includes carrier type and carrier-free type, among which lactose is the only carrier approved by the Food and Drug Administration (FDA) for the preparation of it. At present, lactose with various physicochemical properties in the market can be used for the preparation of DPI with good safety. However, lactose as a carrier has certain limitations (some drugs may have strong absorption of lactose, and lactose is easy to deposit in the oropharynx during administration, resulting in a very small amount of drugs entering the respiratory tract; long-term use of lactose-containing DPI may cause dental caries, etc.) and it is suitable for low doses of drugs. The deposition of drug particles of DPI without carrier type in the lung is not affected by the separation of drug and carrier surface, and can avoid the potential toxic and side effects of carrier on the body, so it is suitable for high dose drugs [25–26]. Among them, L-leucine (LL) is one of the most widely used excidients, which is enriched on the surface of drug particles, reduces the interparticle force, improves the fluidity of dry powder, and improves the dispersion and atomization properties of dry powder [26–28]. In addition, some studies have shown that it can enhance the anti-hygroscopicity of DPI to improve the stability of the drug [26–28]. At present, the preparation of DPI using LL as excipient by spray drying technology has been widely used [26–28]. In this study, Sal B was used as the model drug and LL was used as the excipiant to prepare Sal B-DPI by spray drying. The quality of Sal B-DPI was evaluated by modern preparation evaluation methods. The lung irritation evaluation, *in vivo* and *in vitro* pharmacodynamics, metabolomics, pharmacokinetics and lung tissue distribution were studied to prove the feasibility and rationality of lung administration of Sal B-DPI in the treatment of IPF.

2. Materials and methods

2.1. Materials

Sal B (Lot#:P18J9F65817, purity 98.0%), L-leucine(Lot#:H15J7H17735) were purchased from Shanghai Yuanye Biotechnology Co., Ltd (Shanghai, China). Transforming growth factor-β1 (TGF-β1) was purchased from R&D System (USA). DMEM medium and fetal bovine serum were purchased from Gibco (New York, USA). I Collagen type α1 (COL1A1), III Collagen type α1 (COL3A1), Intercellular adhesive molecule-1, ICAM-1), Arginase type 1 (Arg-1), Fibronectin (FN), Inducible nitric oxide synthase (iNOS) primers were purchased from Shanghai Sangon Bioengineering Co., Ltd. (Shanghai, China). IL-8 ELISA kit was purchased from Shanghai Sinovac Biotechnology Co., Ltd. (Shanghai, China). Total protein quantitative, LDH , SOD activity and MDA assay kit were purchased from Nanjing Jiancheng Biotechnology Co., Ltd. (Nanjing, China). Bleomycin was purchased from Nippon Chemical Co., Ltd. Vegat (nidanib sulfonic acid soft capsule) (C31H33N5O4, 150 mg/capsule, Lot#: 900,678) from Catalent Germany Eberbach GmbH (Germany). IL-1β, IL-6, IL-4, IL-18 and TGF-β1 ELISA kits were purchased from Wuhan Bode Bio-engineering Co., Ltd. (Wuhan, China). IFN-γ, MPO and HYP ELISA kits were purchased from Sinovac Biotech Co., Ltd. (Shanghai, China). Protocatechuic aldehyde (PA), used as internal standard (IS), (Lot#:w06–2–5, purity 98.0%) were purchased from Zhongxin Pharmaceutical Research Center (Tianjin, China). Heparin sodium (batch no. 325D024, titer $\geq$140 units/mg) was purchased from Suolai Bao Technology Co. Ltd (Beijing, China). Formic acid (batch no. K3JHG.LS, purity 98%) was purchased from Chemical Industry Co. Ltd (Tokyo, Japan). HPLC-grade acetonitrile, methanol and phosphoric acid(Lot#:130,271) were purchased from Fisher Scientific Inc. (Fairlawn, USA). Analytical-grade hydrochloric acid was purchased from Jiangtian Chemical Technology Co. Ltd (Tianjin, China). Ascorbic acid (batch no.102045-201,504, purity 98%) was purchased from the National Institutes for Food and Drug Control (Beijing, China). HPLC-grade water was purified using a Milli-Q Reagent Water system (Millipore, Milford, MA, USA).

2.2. Cell lines and animals

NIH-3T3 mouse embryonic fibroblast was obtained from American Type Culture Collection (Maryland, USA). The cells were cultured in high glucose DMEM medium containing 10% fetal bovine serum, 100 mg/l streptomycin and 100 kU/l penicillin, pH 7.2–7.4. The cells were incubated at 37 °C with 5.0% CO_2 atmosphere. Male Sprague–Dawley rats (weighing 170–200 g; Beijing Weitong Lihua Experimental Animal Technology Co., Ltd, Beijing, China; license SCXK 2016–0006) were kept in an environmentally controlled breeding room for 1 week before the experiments. Rats were fasted for 12 h and supplied with unlimited water prior to the experiment. The protocol and any amendments or procedures involving the care or use of animals in this study were in accordance with the regulations for animal experimentation issued by the State Committee of Science and Technology of China and approved by TJUTCM's Institutional Animal Care and Use Committee (document number TCM-LAEC 2,020,055).

2.3. Production of powder formulations by spray dryer

Feed solutions were prepared by dissolving Sal B and LL in water with known mass ratios of Sal B to LL. The feed concentration (total solids content) was maintained at 1.50%. A B-90 nano spray-dryer (Büchi Labortechnik AG, Falwil, Switzerland) was operated under the following parameters [29]: inlet temperature of 80 °C, air flow of 100 l/min, pump speed of 23%, spray rate of 60%, and internal pressure of 34 Mbar. After the above parameters were stabilized, the spray would begin. The spray-dried powders were stored in a desiccator containing silica gel at room temperature without light until used.

2.4. Quality evaluation of spray-dried powders

2.4.1. Particle sizing of spray-dried powders
The volumetric diameter and span of the sample powders were analyzed by a laser particle size analyzer (HELOS (Hi214) & OASISDRY, R1; Sympatec GmbH, Goslar, Germany) [30]. The parameters of D_{10}, D_{50}, D_{90} and volume surface mean diameter were separately determined, representing the sizes at which 10%, 50%, and 90% of the particles were smaller than the remaining particles and the mean volume diameter.

2.4.2. Scanning electron microscopy (SEM)
SEM (JSM-7500F; JEOL Int., Tokyo, Japan) was employed to examine particle morphology of the powder formulations at 10 kV. The samples were coated with a layer of gold and dried in a vacuum [26].

2.4.3. X-ray powder diffraction (XRD)
Powder crystallinity was evaluated by XRD (D/MAX-2550 V; Rigaku Int., Tokyo, Japan), using Cu Ka radiation at a voltage of 40 kV and a current of 30 mA. Data were recorded from 5°−50° (2θ) using a scan speed of 2 per min and a step size of 0.02 [26].

2.4.4. Dynamic vapor sorption (DVS)
A DVS instrument (Surface Management Systems, London, United Kingdom) was used to derive the moisture sorption isotherms of sample powders. The chamber was kept at 25 °C under continuous nitrogen flow. 30–50 mg of each sample was dried at 0 RH for 1 h before being exposed to one cycle of 0–90% RH, with 10% RH increments. After the sample gradually reached the moisture absorption balance at each relative humidity, the next level of relative humidity test would be automatically performed [26].

2.4.5. Content determination
The content of Sal B in spray-dried powders of various mass ratios were determined by HPLC according to the chromatographic conditions in the Supplementary material.

2.4.6. In vitro aerosol performances
A next-generation pharmaceutical impactor (NGI-1302; Copley Scientific, Nottingham, UK) was used to evaluate the aerosolization behavior of spray-dried powders with a United

States Pharmacopoeia (USP) induction port. An ethanol solution containing a certain amount of benzyl and glycerin was added to the surface of each collection cup and then evaporated at ambient temperature for 2 h to avoid particle bounce or re-entrainment. Spray-dried powders were loaded into an Easyhaler multiple dose powder inhaler (Orion Int., Espoo, Finland). The test was carried out (4 s, 60 l/min flow rate). Five shots were fired into Next Generation Impactor (NGI) for each formulation. Thoroughly rinse all stages with a predetermined volume of water after aerosolization. The collected solutions were analyzed by HPLC as content determination.

The parameters of aerosol properties were calculated by CITDAS software (version 3.00; Copley Scientific): fine particle dose (FPD), fine particle fraction (FPF), mass median aerodynamic diameter (MMAD) and geometric standard deviation (GSD). FPD refers to the dose of drug particles with aerodynamic diameter of < 5 μm, whereas FPF is defined as the ratio of FPD to the total recovery dose [31]. In addition, delivery efficiency refers to the ratio of the amount of powder collected in each part of the NGI to the total dose.

2.5. Preliminary stability investigation

The Sal B-DPI(80SalB20LL) was stored in a desiccator containing silica gel at room temperature without light. The temperature and humidity corresponding to this condition are 20 ± 2 °C and $20\% \pm 2\%$, respectively. Samples were taken on Day 1 and 35 for particle size distribution, morphology, XRD analysis, content determination and in vitro aerodynamics analysis.

2.6. Anti-pulmonary fibrosis in vitro

2.6.1. MTT assay
MTT assay was used to verify whether these isolates had toxic side effects on normal fibroblasts and the effect on vitality of fibroblasts [32]. NIH-3T3 mouse embryonic fibroblasts (Normal fibroblasts) were plated in 96-well plates, and each compound was set to a concentration gradient of nidanib (0.25, 0.5, 1, 2.5, 5 and 10 μM) and Sal B-DPI(80SalB20LL) (25, 50, 100, 125, 150, 175 and 200 μg/ml). After incubation for 48 h, 20 μl MTT solution (5 mg/ml) was added to each well, and the culture was continued for 4 h. After that, 110 μl DMSO was added to each well, and the absorbance value of each well was measured at 490 nm with a microplate analyzer.

2.6.2. Sirius red method
The effect of Sal B-DPI on collagen deposition in NIH-3T3 cells induced by TGF-β1 was determined by Sirius red method [33]. The optimal stimulating dose of TGF-β1 was 5 ng/ml. SB431542, a selective inhibitor of TGF-β1 signaling, was used as a positive control at a concentration of 5 μM. Each compound was set to a concentration gradient of nidanib (0.25 μM and 0.5 μM) and Sal B-DPI (25, 50 and 125 μg/ml). After incubation for 48 h, Sirius red 100 μl was added to each well and kept away from light at room temperature for 4 h. The detection was performed at 540 nm.

2.6.3. Scratch test
NIH-3T3 mouse embryonic fibroblasts were coated with 12-well plates and cultured for 24 h and then scratched [34]. After 24 h of synchronization, 5 ng/ml TGF-β1 and drugs (SB431542, nidanib, Sal B-DPI) were added and incubated for 48 h. Photographs were taken with an inverted microscope at 0, 24 and 48 h after drug addition, respectively.

2.6.4. qPCR detection [31–34]
NIH-3T3 mouse embryonic fibroblasts were coated with 6-well plates and cultured for 24 h. 5 ng/ml TGF-β1 and Sal B-DPI(50 μg/ml) were added and incubated for 48 h. RNA was extracted from cells for qPCR, and the expressions of COL1A1, COL3A1, ICAM-1, FN, iNOS and Arg-1 were detected to analyze the activation degree of NIH-3T3. Primer sequences are shown in Table S1.

2.7. Pulmonary irritation

2.7.1. Grouping and administration
18 experimental rats were fed adaptive for 3 d The rats were divided into 3 groups by random number expression method: normal control group (NC), sham operation group (sham), and pulmonary administration of Sal B-DPI (80SalB20LL) group(Sal B-DPI), with 6 rats in each group. SD rats in Sal B-DPI group were anesthetized and fixed by intraperitoneal injection of 10% chloral hydrate (2 ml/kg). SD rats were administrated with 10 mg/kg of Sal B-DPI by the method described below [35–36]. The method was as follows: Sal B-DPI was loaded into a DP-4R dry powder injector and equipped with an SC-X sample chamber dilator (Penn Pancentury, Inc., Wyndmoor, PA). The delivery tube of the inhaler had been carefully introduced into the trachea before the first trachea bifurcated. 1.5 ml air corresponding to the tidal volume of SD rats was pumped to Sal B-DPI at a relatively steady rate for three consecutive times. The sham group was administered in the same manner as Sal B-DPI group, except that no Sal B-DPI was administered.

2.7.2. Sample collection and preservation
The sample collection method is optimized based on the previous research, especially the collection of broncho alveolar lavage fluid(BALF) [14,16]. After weighing, the rats in the three groups were anesthetized by intraperitoneal injection of 10% chloral hydrate (2 ml/kg). The rats were sacrificed after blood collection through abdominal aorta. After the tracheal branch was found, the left lung of the rats was ligated with a hemostatic clip. A small incision was cut near the tracheal branch, and a plastic tube was inserted into the right bronchus along the incision, which was immediately fixed with a sterile surgical thread, and the lavage operation was ready to begin. 2 ml normal saline at 4 °C was taken with a sterile syringe and slowly injected into the right lung of rats through the three-way valve of the retained needle. The normal saline remained in the lung tissue for 1 min, and the lavage fluid was slowly withdrawn. After repeated lavage for 3 times, the lavage fluid was collected and mixed in ice bath. After lavage, the lung tissue was separated, the surface of the lung tissue was rinsed with normal saline and dried with filter paper. The left lung of the rats was soaked in 10% neutral

formalin solution and fixed at room temperature for 48 h, then used for pathological observation of lung tissue.

2.7.3. Determination of total protein, IL-8 concentration and lactate dehydrogenase (LDH) activity in BALF

Total protein, IL-8 and LDH activity in the supernatant of BALF in each group were quantitatively determined by BCA method, enzymatic linked immunosorbent assay (ELISA) and microplate method, respectively, according to the kit instructions.

2.8. Preliminary pharmacodynamics study in vivo

2.8.1. Rat model of IPF

After the experimental rats were anesthetized by intraperitoneal injection of 10% chloral hydrate (2 ml/kg), 0.1 ml bleomycin saline solution (5 mg/kg) was injected into the trachea through the space of the tracheal cartilage ring into the rat's lungs. Immediately place the rat upright and rotate it for 5 min to make the solution evenly distributed in the rat's lungs [14,16].

2.8.2. Grouping and administration

30 experimental rats were fed adaptively for 3 d They were divided into 5 groups by random number expression, normal control group (NC), bleomycin group (bleo), and pulmonary administration of Sal B-DPI (80SalB20LL) group (bleo+Sal B-DPI), intravenous injection of Sal B solution group (bleo+Sal B iv) and intragastric administration of positive drug nidanib group (bleo+nidanib) .

The NC group was injected with equal volume of normal saline in the way of tracheal non-invasive pulmonary administration, and the other groups were injected with bleomycin normal saline solution to induce the rat model of IPF. The model was established as the 0 d of the experiment. Each treatment group was given drug intervention on the 1st d. The bleo+Sal B-DPI group was given Sal B-DPI (10 mg/kg, measured by SalB) by the method described in "2.7.1" for 28 d, once a day. The bleo group was pushed into air as described above. Rats in the bleo+Sal B iv group were injected with Sal B solution at the same dose as those in the bleo+Sal B-DPI group. The positive drug nidanib was administrated intragastrically with a dose of 31.5 mg/kg (measured by nidanib). During administration, activities, breathing, feeding, hair and body weight of rats in each group were observed carefully every day.

2.8.3. Non-invasive lung function measurement

On Day 29, the system of drug administration and respiratory physiological detection for awake animals was started. After the equipment was calibrated, rats in each group were placed into the animal plysmography chamber in batch. When the rats were in normal state and breathing was stable, various indicators of lung function including tidal volume (TV), minute volume (MV). After the measurement, further specimen collection was carried out. TV: The volume of air inhaled or exhaled with each breath is an indicator of lung volume of lung function in rats; MV: The total amount of gas inhaled or exhaled per minute, which is also the product of TV and respiratory frequency, is one of the ventilation indicators of lung function in rats.

2.8.4. Sample collection and preservation

On Day 29, rats in each group were sacrificed, and serum, BALF and lung tissue were collected. After weighing, the rats in the three groups were anesthetized by intraperitoneal injection of 10% chloral hydrate (2 ml/kg). The rats were sacrificed after blood collection through abdominal aorta. The procedure for collecting BALF was the same as "2.7.2". After lavage, the lung tissue was separated, the surface of the lung tissue was washed with ice normal saline, and the water on the surface of the lung tissue was dried with filter paper. Part of the left lung of the rats was soaked in 10% neutral formalin solution, fixed at room temperature for 48 h, and then used for staining of the lung tissue sections. Part of the left lung was stored at −80 °C for the determination of Hyp, SOD activity and MDA content [37].

2.9. Metabonomics study of lung tissue in rats

2.9.1. Processing of lung tissue samples

According to a weight-to-volume ratio of 1:5 (g/ml), physiological saline was added to the lung tissues of each group in an appropriate amount, and placed in an ice-water bath to prepare a homogenate. Take 200 μl lung tissue homogenate, add 4 times the amount of methanol, vortex for 2 min, and centrifuge at 12 000 rpm at 4 °C for 10 min. Take the supernatant, dry it with nitrogen at room temperature, add 100 μl methanol for reconstitution, and centrifuge at 4 °C at 12 000 rpm for 10 min. The supernatant was injected and UPLC-Q-TOF/MS liquid mass spectrometry was used to analyze the difference components in each group. The UPLC-Q-TOF/MS analysis conditions were described in the Supplementary material

2.9.2. Metabonomics data processing [38]

Import the Raw. data after sample injection and analysis based on QI software (Waters, USA). Based on the software's automatic identification function, complete basic operations such as feature extraction of batch samples, QC feature standardization, chromatographic peak alignment, peak matching, retention time correction, etc. Export a list of all chromatographic peaks in the form of an Excel table, mainly including: RT, *m/z*, MS/MS, S/N, standardized peak area and other related parameters.

Then, on the basis of the original table, analyze the number of "0 values" in each group, and further eliminate and improve irrelevant data according to relevant rules. The candidate differential metabolites were screened based on the VIP value of multivariate statistical analysis, and statistical analysis was carried out by parametric test according to the data type and specific distribution.

Using the precise molecular weight *m/z* of high resolution mass spectrometry, it can be found in HMDB database (http://www.hmdb.ca/), Chemspider database (http://www.chemspider.com/), Metlin (http://metlin. scripps.edu) to find possible endogenous components, combined with MS/MS and molecular error (ppm) to determine the final differential molecule.

In order to illustrate the role of differential metabolites in organisms, this article conducts pathway enrichment analysis for all metabolites on the open source website MetPA

(https://www.metaboanalyst.ca/). Screen the biologically significant metabolites and analyze the metabolic pathways where the metabolites accumulate, and find out the potential pathways for Sal B-DPI in the treatment of IPF.

2.10. Preliminary pharmacokinetics and lung tissue distribution study

2.10.1. Preliminary pharmacokinetic study
Twelve male Sprague-Dawley rats (200 ± 20 g) were randomly divided into two groups ($n = 6$ per group). For Sal B-DPI group, Sal B-DPI (10 mg/kg, measured as Sal B) was administered to the lung by the method under "2.7.1". In another group, the same dose of Sal B solution was intravenously administered. Blood samples (0.5 ml) were immediately collected in heparinized 1.5 ml polythene tubes from the suborbital vein at 0.033, 0.083, 0.25, 0.5, 1, 2, 4, 6 and 12 h after administration. Blood samples were immediately centrifuged at 3000 rpm (Thermo Fisher, Massachusetts, USA) for 10 min at 4 °C to obtain plasma. All of the plasma samples were kept at −80 °C until analysis.

Each plasma sample (100 μl) was spiked with 10 μl ascorbic acid solution (1.4 mg/ml in water), 100 μl IS working solution (0.98 μg/ml PA), 20 μl hydrochloric acid (2 mol/l in water) and 1 ml ethyl acetate and briefly vortex-mixed for 2 min, centrifuged (12 000 rpm) for 10 min and the supernatant separated. The supernatant was carefully transferred into another tube, dried with nitrogen and diluted with 100 μl methanol-water (80:20, v/v), vortex-mixed for 2 min and centrifuged (12 000 rpm) for 10 min. Finally, 3 μl the supernatant was injected into the UPLC-MS/MS system for analysis [39]. The specific methods were presented in supplementary materials. The relevant pharmacokinetic parameters were determined using the plasma concentration-time data and calculated by WinNonlin version 6.4 (Pharsight Corporation, Mountain View, CA). The method was developed and validated with respect to specificity, linearity, precision, accuracy, recovery, matrix effect, and stability through the processing procedure and sample storage.

2.10.2. Lung tissue distribution study
Fifty-four male Sprague-Dawley rats (200 ± 20 g) were randomly divided into two groups (pulmonary administration group and intravenous administration group). Each group has 9 time points of 0.033, 0.083, 0.25, 0.5, 1, 2, 4, 6 and 12 h ($n = 3$ per time point). For Sal B-DPI group, Sal B-DPI (10 mg/kg, measured as Sal B) was administered to the lung by the method under "2.7.1". In the another, the same dose of Sal B solution was intravenously administered. After the administration of 0.033, 0.083, 0.25, 0.5, 1, 2, 4, 6, and 12 h later, the rats were sacrificed via the abdominal aorta and lung tissue was collected. All of the samples were kept at −80 °C until analysis.

According to the weight to volume ratio of 1:5 (g/ml), an appropriate amount of lung tissue was added to normal saline, and homogenate was prepared under the condition of ice water bath. The lung tissue homogenate processing method was the same as the plasma sample processing method under "2.10.1". The relevant pharmacokinetic parameters were determined using the concentration-time data and calculated

by WinNonlin version 6.4 (Pharsight Corporation, Mountain View, CA). The method was developed and validated with respect to specificity, linearity, precision, accuracy, recovery, matrix effect, and stability through the processing procedure and sample storage.

2.11. Statistical analysis

Statistical software SPSS 23.0 was used for statistical analysis, and measurement data was expressed as mean $\pm$ SD. One-way ANOVA was used for comparison among groups. $P < 0.05$ indicated significant difference, $P < 0.01$ indicated extremely significant difference. $P > 0.05$ indicated no significant difference. All data were mapped using GraphPad Prism 8 software and Adobe Illustrator CS6 software.

3. Results and discussion

3.1. Quality evaluation of spray-dried powders

3.1.1. Particle size analysis
The particle size distribution data of powder formulations are summarized in Table 1. Most particles of each formulation were smaller than 5 μm, suitable for DPI formulation [40]. The D_{50} values of pray-dried (SD) pure Sal B and pure LL were 1.42 μm and 2.35 μm, while the co-spray dried formulations had fairly similar D_{50} values around 1.10 μm (range 1.00–1.17 μm).

3.1.2. Particle morphology
SEM images of various formulations were shown in Fig. 1A, which confirmed the particle size data presented in Table 1, with the majority of particles being < 5 μm diameter. The surface roughness of SD Sal B particles increased with the amount of LL, most obviously in the sample containing 20% (w/w) LL. The formulations were made up of spherical or nearly spherical particles with a corrugated surface and hollow particles with a smooth surface. This could be due to the enrichment of LL on the surface of the drug particles, thereby reducing the force between them, improving the fluidity, dispersion and atomization performance of DPI [41]. The crystallinity of LL in various formulations would be discussed below.

3.1.3. Crystallinity
The raw material of LL exhibited a distinct diffraction peak in Fig. 1B-1, wheras Sal B did not. SD LL was crystalline, with peaks around 6°, 12°, 20°, 25°, 31°, 34° and 38° In contrast, powders containing both Sal B showed only a broad peak at about 20°, suggesting that the powder was mostly amorphous (Fig. 1B-2). During long-term storage, amorphous powders may gradually change to crystalline form . As a result, storage conditions for Sal B-DPI should be monitored(temperature, humidity, etc.).

3.1.4. DVS
At 0–90% RH, SD Sal B alone absorbed a significant amount of water. According to hygroscopicity classification systems, SD Sal B is very hygroscopic which is partly due to the amorphous
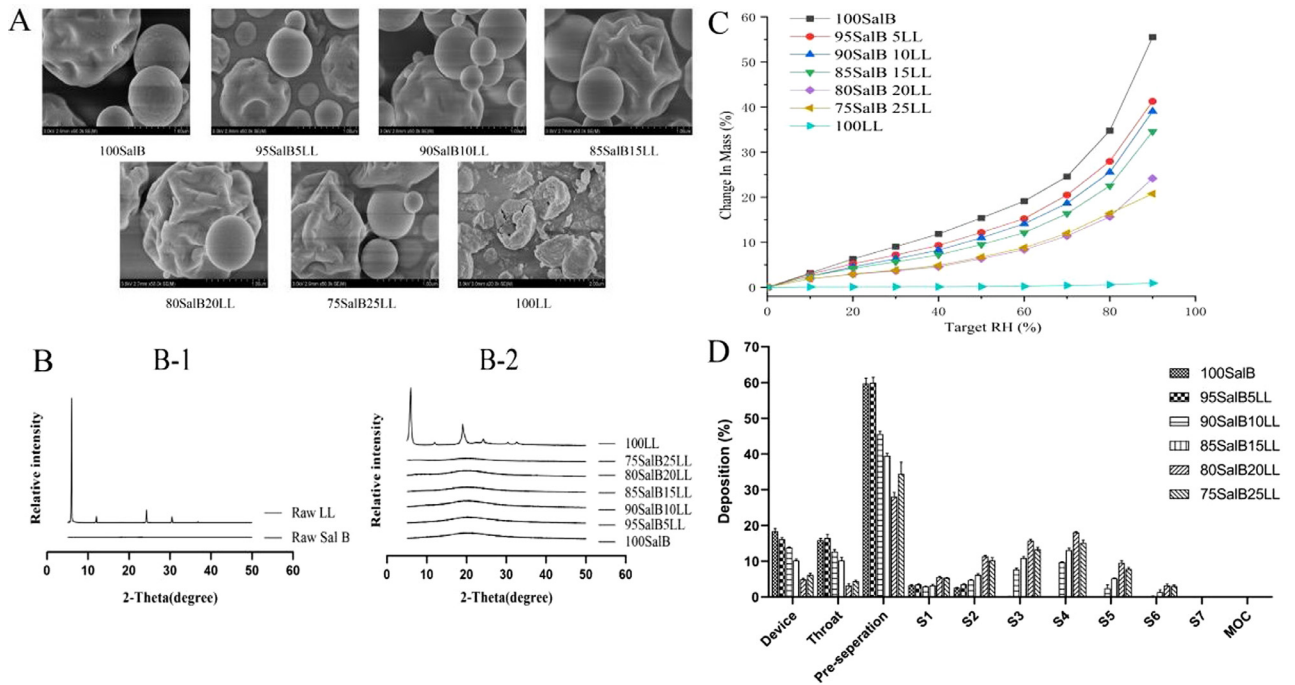
Fig. 1 – Quality evaluation of spray-dried powders. (A)SEM images of SD Sal B-LL particles. (B)X-ray powder diffraction patterns of (B-1) raw powders and (B-2) spray-dried formulations containing Sal B and LL. (C)Hygroscopicity diagram of spray-dried formulations containing Sal B and LL. (D)The effect of amounts of LL on *in vitro* aerosolization performances of Sal B-LL composite powders($n = 3$).
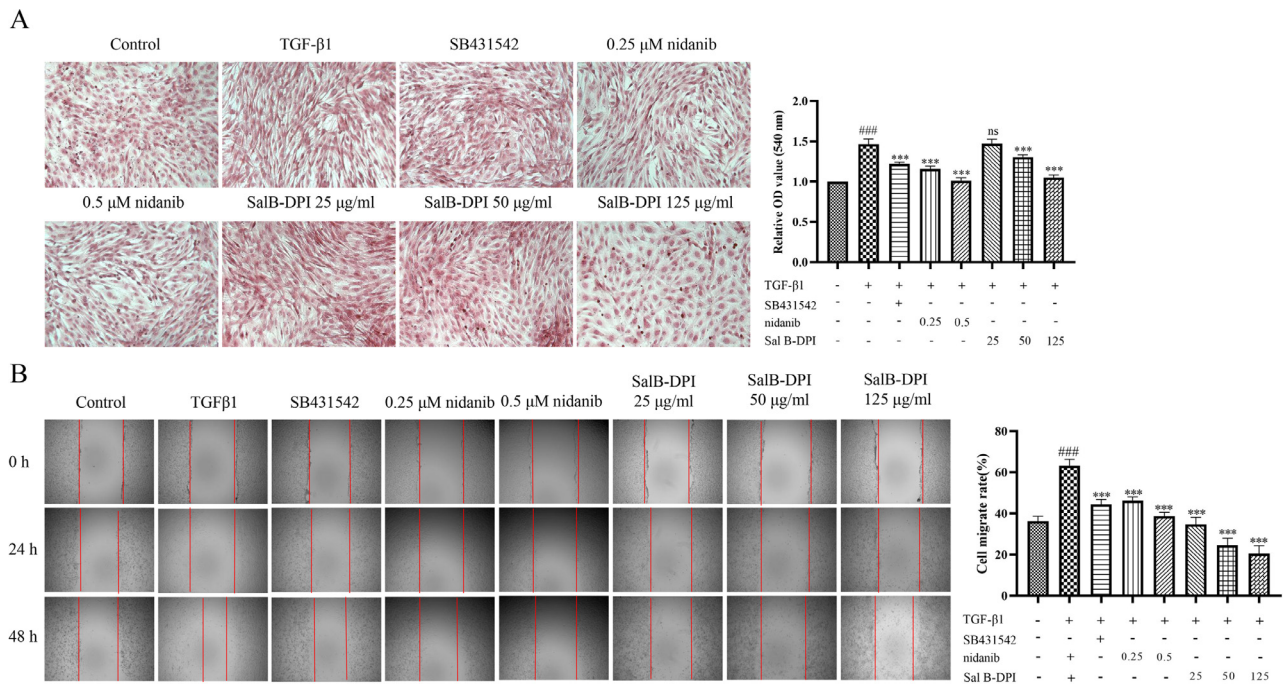

Fig. 2 – Effect of TGF-β1 on collagen content of NIH-3T3 cells(A)and effects of TGF-β1 on NIH-3T3 cell migration(B). $^{###}P < 0.001$ vs control group, $^{***}P < 0.001$ vs TGF-β1 group.

Table 1 – Particle size distributions of various formulations($n = 3$).

Formulations[a]	D_{10}/µm	D_{50}/µm	D_{90}/µm	VMD/µm
100SalB	0.36±0.03	1.42±0.10	2.56±0.12	1.47±0.08
95SalB5LL	0.33±0.01	1.09±0.01	2.02±0.03	1.15±0.01
90SalB10LL	0.34±0.00	1.11±0.01	2.11±0.05	1.19±0.02
85SalB15LL	0.33±0.01	1.17±0.01	2.27±0.04	1.25±0.02
80SalB20LL	0.34±0.01	1.15±0.01	2.16±0.02	1.22±0.01
75SalB25LL	0.38±0.01	1.00±0.01	1.87±0.01	1.08±0.01
100LL	0.91±0.01	2.35±0.05	5.10±0.17	2.72±0.07

    [a] The codes "100Sal B" and "100LL" represent 100% (w/w) Sal B and LL, respectively; "95SalB5LL" represents 95% (w/w) Sal B and 5% (w/w) and so on.

Table 2 – Content of Sal B in various formulations and results of *in vitro* deposition properties .

Formulations	Sal B%	DE(%)	MMAD(µm)	GSD	FPF/%	FPD/mg
100SalB	99.32±0.68	73.57±0.37	NA	NA	0.48±0.06	0.02±0.00
95SalB5LL	94.24±0.55	75.25±2.15	7.81±0.06	1.42±0.02	0.75±0.13	0.03±0.00
90SalB10LL	89.69±0.68	78.26±1.14	3.07±0.10	2.10±0.03	21.35±0.92	0.96±0.05
85SalB15LL	84.76±0.15	85.85±1.39	2.85±0.07	1.99±0.02	32.18±0.33	1.41±0.30
80SalB20LL	79.39±0.70	90.43±0.31	2.88±0.02	2.09±0.04	49.71±0.90	2.36±0.07
75SalB25LL	74.56±0.29	83.76±1.37	2.94±0.01	2.14±0.02	42.02±1.84	1.95±0.06

DE: delivery efficiency; Sal B%: content of Sal B.

form of Sal B, as confirmed by XRD. In contrast, SD LL alone was crystalline and non-hygroscopic, with less than 1% water absorbed. Thus, the contribution of water uptake of LL in the composite powders would be negligible. As LL was added to the formulations, the water uptake at elevated RH was decreased with increasing amounts of LL. It was discovered that LL could enhance the anti-hygroscopicity of DPI to a certain extent, thereby improving the stability of the drug. The hygroscopic behavior of 80SalB20LL and 75SalB25LL was similar when RH was 0–80%, and the hygroscopic behavior of 80SalB20LL was slightly stronger when RH was 80%−90% (Fig. 1C).

3.1.5. Content determination
The content determination results of Sal B-DPI with various fomulations were shown in Table 2. The content of Sal B is 99.32%, 94.24%, 89.69%, 84.76%, 79.39% and 74.56%, respectively.

3.1.6. In vitro aerosol performances
The results of *in vitro* deposition properties of various formulations were shown in Table 2 and Fig. 1D. The delivery efficiencies of SalB-DPI with various fomulations were all greater than 70%, and the FPF value ranged from 0.48% to 49.71%, with the FPF value reaching the maximum when the LL content was 20%. With the addition of LL increasing, the *in vitro* deposition properties of DPI were improved [42]. Among the six formulations mentioned above, 80SalB20LL had the most obvious surface roughness, particle size less than 3 µm, relatively strong hygroscopic resistance, the highest delivery efficiency and the largest FPF value, and the best deposition effect *in vitro*. Therefore, 80SalB20LL was selected for the preliminary stability test and subsequent test.

On the basis of previous studies [41], the diameter of DPI was reduced from 8 µm to 3 µm by replacing the nozzle of B-90 spray dryer, and the particle size distribution was more uniform, so as to further improve the deposition efficiency of drugs *in vitro*. Similarly, the FPF value of 80SalB20LL increased from 37.55% to 49.71%. Other studies on Salvia miltiorrhiza related dry powder inhalers mainly adopted grinding method, with drug delivery efficiency less than 86.00% and FPF value less than 46.00% [43]. In this experiment, the drug delivery efficiency of 80SalB20LL dry powder inhaler was 90.43%, and the FPF value was 49.71%. Moreover, the preparation method and prescription composition were convenient and simple, which provided reference for the preparation of DPI of traditional Chinese medicine.

3.2. Preliminary stability investigation

The particle size of Sal B-DPI(80SalB20LL) stored in the brown dryer at room temperature on Day 1 and 35 was less than 3 µm (Fig. S1A). With the increase of time, the surface roughness of particles did not increase significantly (Fig. S1B). The 80SalB20LL stored in the brown dryer at room temperature on Day 1 and 35 was mainly amorphous and did not crystallized (Fig. S1C). The content of Sal B in Sal B-DPI stored at room temperature on Day 1 and 35 was 79.39% ± 0.70% and 79.08% ±0.39%, respectively, without significant change (Fig. S1D). The *in vitro* deposition properties of Sal B-DPI stored at room temperature on Day 1 and 35 were shown in Fig. S1E. The deposition of Sal B at various levels of NGI was shown in Fig. S1F. The delivery efficiency of Sal B-DPI on Day 1 and 35 were 90.13% ± 0.46% and 89.85% ± 0.82)%, respectively, and the FPF values were 49.05% ± 0.30% and 47.96% ± 0.95%, respectively. After 35 d, the deposition rate *in vitro* decreased slightly, but

there was no significant difference. The above indicated that Sal B-DPI stored in the brown dryer at room temperature was stable for 35 d

3.3. Anti-pulmonary fibrosis in vitro

3.3.1. MTT assay

NIH-3T3 cells are commonly used cell lines for *in vitro* experiments in cell-level experiments to investigate fibrosis. During the development of fibrosis, some fibroblasts differentiate into myofibroblasts and produce and accumulate excessive collagen, and the deposition of collagen will destroy the structure and function of lung tissue, thus triggering fibrosis [44]. In this study, SalB-DPI(80SalB20LL) containing 79.39% Sal B was selected as therapeutic agent. MTT assay was used to detect the effects of nidanib and Sal B-DPI on NIH3T3 cell proliferation. The results showed that nidanib ($< 1\,\mu M$) and Sal B-DPI ($< 125\,\mu g/ml$ d no significant effect on cell viability. Therefore, nidanib (0.25 and $0.5\,\mu M$) and Sal B-DPI (25, 50 and $125\,\mu g/ml$ were selected for subsequent experiments(Fig. S2).

3.3.2. Effect of TGF-β1-induced collagen content in NIH-3T3 cells

In the injury and repair stage of pulmonary inflammation, macrophages would participate in the regulation of inflammatory response, secreting transforming growth factor TGF-β1, etc., which further stimulated the proliferation of fibroblasts, resulting in remodeling of extracellular matrix (ECM), excessive deposition of collagen, and the development of irreversible pulmonary fibrosis. In this study, Sirius red staining was used to detect intracellular collagen deposition after TGF-β1-induced activation to confirm the successful induction of the cell model and to use it as a cell model for collagen deposition in IPF [44]. As can be seen from Fig. 2A, collagen content in cells significantly increased (red area significantly increased) 48 h after TGF-β1 induction, and the occurrence of this process was inhibited by the positive drug group (SB431542). Compared with TGF-β1 group, nidanib significantly inhibited the increase of collagen content in a concentration-dependent manner. When the concentration of Sal B-DPI was greater than $50\,\mu g/ml$ it had a significant inhibitory effect on collagen content in NIH-3T3 cells in a concentration-dependent manner. The inhibitory effect of $125\,\mu g/ml$ Sal B-DPI on collagen content was similar to that of $0.5\,\mu M$ nidanib.

3.3.3. Effect of TGF-β1-induced NIH-3T3 cell migration

As shown in Fig. 2B, NIH-3T3 cells migrated significantly after 48 h induced by TGF-β1 compared with the blank group, and SB431542 significantly inhibited the process. Compared with the TGF-β1 group, both nidanib and Sal B-DPI significantly inhibited the migration of NIH-3T3 cells in a concentration dependent manner.

3.3.4. Effect of TGF-β1-induced NIH-3T3 cell activation

Current studies have shown that IPF was associated with stages of oxidative stress, inflammatory response and fibrosis. In recent years, studies on the pathogenesis of IPF have not been limited to the pathogenesis of alveolar inflammation,

which may be caused by endogenous and exogenous cellular stress, resulting in fibroblast activation, alveolar structural damage and ECM protein deposition, etc., and further causing gas exchange disorders and respiratory failure. In the course of its pathogenesis, macrophages run through the whole pathogenesis, and different phenotypes have different effects on it [45]. The polarization of macrophages is regulated by microbial signals, tissue-specific induction and cytokines, and the polarization of different subtypes is regulated by different signaling pathways. In different stages of pulmonary fibrosis, the two types of cells are polarized to different subtypes, and their polarized phenotypes include M1-type macrophages and M2-type macrophages [45]. M1-type macrophages secrete iNOS as one of the nitric oxide synthase (NOS), and under normal circumstances, iNOS is almost not expressed in all tissues and cells, but under pathological conditions, it can be induced and activated by some cytokines, leading to the increase of NO content, and then affecting some pathological processes [46]. i NOS and its product NO promote the occurrence of pulmonary fibrosis by participating in the oxidative stress injury of lung tissue. As an important enzyme in arginine metabolism, Arg-1 catalyzes the denitrification of arginine into ornithine, which is an essential precursor molecule for collagen synthesis. Under the regulation of type 2 helper T cell (Th2) cytokines, Arg-1 can be highly expressed in type M2 macrophages. It was found that overexpression of Arg-1 significantly increased bleomycin-induced pulmonary fibrosis in mice [47]. The TGF-β1/Smad signaling pathway plays an important role in the process of cell polarization, and the accumulation of TGF-β1-mediated ECM precipitation is a Smad3-dependent process. FN, COL1A1 and COL3A1 are the main components of ECM. Excessive deposition of FN, COL1A1 and COL3A1 can lead to scarring, pulmonary dysfunction, respiratory failure, and ultimately death [48–49]. ICAM-1 belongs to a family of immunoglobulins that regulate cell-to-cell and cell-ECM interactions. The main receptor of ICAM-1 was Lymphocyte function-associated antigen-1 (LFA-1), which was mainly expressed in the inflammatory cells such as eosinophils, neutrophils and T lymphocytes. The interaction between ICAM-1 and LFA-1 caused the above inflammatory cells to adhere to vascular endothelial cells and infiltrate the diseased bronchus. In addition, during lung injury, ICAM-1 was highly expressed in pulmonary vascular endothelial cells, leading to adhesion of inflammatory cells to the vascular endothelium and mediating its transendothelial metastasis. At the same time, the high expression of ICAM-1 in the alveolar epithelium also led to the connection of ICAM-1 with activated T cells and multinucleated leukocytes in the alveolar lumen, which led to the development of alveolar inflammation, and further increased the expression of ICAM-1 in inflammatory cells and alveolar epithelium [35].

In order to detect the mRNA expression of TGF-β1 on fibrosis markers of NIH-3T3 cells, fibrosis related factors such as COL1A1, COL3A1, ICAM-1, FN, iNOS and Arg-1 were detected respectively. As shown in Fig. 3, TGF-β1 could significantly increase the expression of fibrosis related factors in NIH-3T3 cells, but the intervention of Sal B-DPI ($50\,\mu g/ml$) significantly reduced the expression of fibrosis related factors.
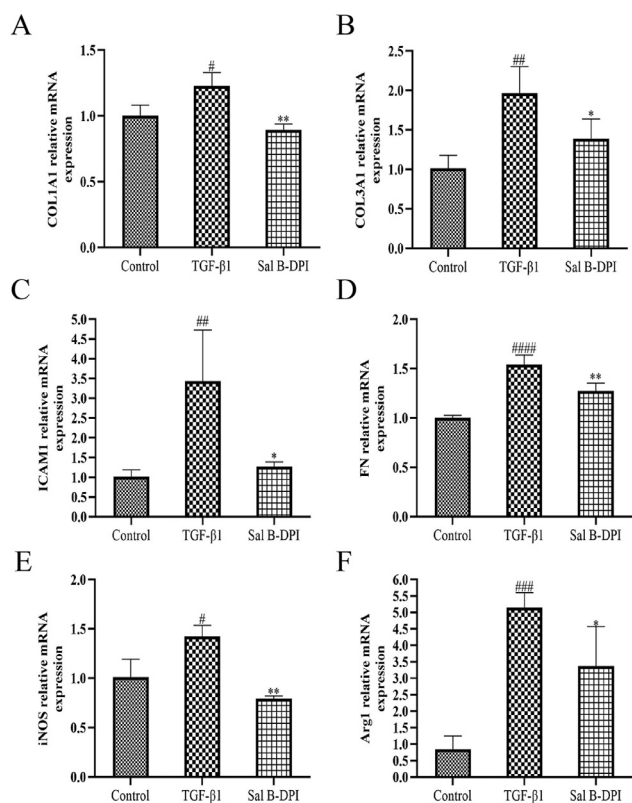
Fig. 3 – Effects of TGF-β1-induced fibrosis related factors in NIH-3T3 cells. (A-F)mRNA expression of COL1A1, COL3A1, ICAM-1, FN, iNOS, and Arg-1. $^{\#}P < 0.05$, $^{\#\#} P < 0.01$, $^{\#\#\#} P < 0.001$, $^{\#\#\#\#} P < 0.0001$ vs control group, $^{*}P < 0.05$, $^{**}P < 0.01$ vs TGF-β1 group.

Fig. 4 – Pulmonary irritation. (A) Hematoxylin & eosin (H&E) staining of rat lung tissue (×200). (B) The concentrations of total protein, IL-8 and LDH in BALF. $^{*}P < 0.05$ vs NC group.

3.4. Pulmonary irritation

The rats in normal control group (NC), sham operation group (sham) and Sal B-DPI group all responded sensitively with good mental status, stable breathing, good diet, fat body, shiny fur and significant weight gain.

The lung tissues of rats in the NC group, sham group and Sal B-DPI group were intact and clear, with thin alveolar walls, no bleeding points, and no inflammation in the alveolar cavity cells infiltrated and exudated, with less collagen deposition(Fig. 4A).

When lung injury and inflammation occurred, inflammatory cells, cytokines and related enzymes in the BALF were abnormally increased. IL-8 is a chemotactic cytokine and an important mediator of inflammatory diseases. IL-8 can chemotactic and activate neutrophils, and then participate in the pulmonary inflammatory response and local lung injury [50]. LDH is widely present in the cytoplasm of all tissues and cells of the body. In normal lung tissues, LDH is mainly derived from the active secretion of lung epithelial cells and the decomposition and release of exfoliated cells. However, in damaged lung tissue, the mucosal integrity of the airway epithelium is affected, resulting in elevated LDH enzyme expression [51]. The total protein concentrations in BALF in NC group and Sal B-DPI group were
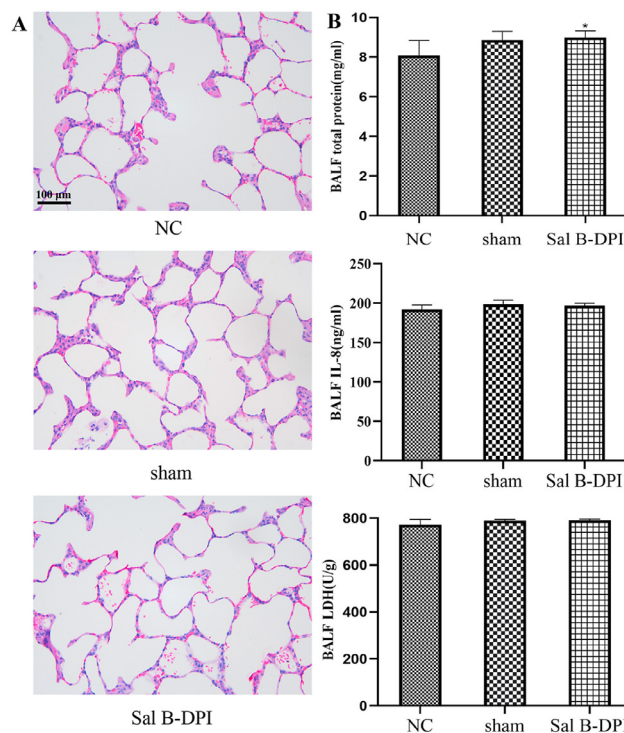
8.08±0.76 and 8.99±0.33 mg/ml, respectively, and there was a significant difference between them ($P < 0.05$). There was no significant difference in the concentration of IL-8 and LDH activity in BALF between the three groups, indicating that the noninvasive tracheal administration is safe, and the lung injury is relatively small. Sal B-DPI may cause slight irritation to the lungs(Fig. 4B).

3.5. Preliminary pharmacodynamics study in vivo

As a glycoside antibiotic, bleomycin is mainly used in the clinical treatment of tumors, but there are obvious adverse reactions of pulmonary interstitial fibrosis, so it is often used to induce pulmonary fibrosis animal models. The histological changes of bleomycin-induced rat model of IPF are very similar to those of human IPF and can well reflect the pathological characteristics of human pulmonary fibrosis [52]. In the experiment of establishing animal model, lung injury after bleomycin administration mainly experienced three different stages:(1) The first 7 d were in the stage of acute injury and inflammation. Due to more epithelial cell damage and increased vascular permeability, a large number of inflammatory cytokines were released and the number of inflammatory cells increased; (2) From the 7th d to the 14th d, it was in the transitional stage from inflammation to active pulmonary fibrosis, during which the inflammatory response gradually subsided, accompanied by a gradual increase in myofibroblast generation and collagen deposition; (3) From Day 14 to 28, chronic pulmonary fibrosis occurs, with obvious forms of alveolar and septal fibrosis, characterized by an

increase in the number of myofibroblasts and the deposition of extracellular matrix. Generally, about 28 d after bleomycin administration, the degree of collagen deposition in the lungs reaches its peak. Bleomycin was widely used to establish animal models of IPF because it can cause pulmonary inflammation and fibrosis in the short term [52]. In this study, the rats model of IPF was induced by one-time infusion of bleomycin normal saline through trachea, and the whole course of administration was used for intervention.

The rats in the NC group are sensitive, and have good mental state, stable breathing, good diet, plump body, shiny fur, and significant weight gain. In the early stage, the modeled rats in other groups were poor in spirit, short of breath, wheezing, slow movements, sparse fur, dull fur, and severe shedding. The rats in the bleo group are in the worst condition, with a significant decrease in food intake, a decrease in drinking water, and an insignificant weight gain. After 7 d in the other treatment groups, the state of rats gradually improved, the breathing became stable, and the weight gradually increased, which was significantly better than the bleo group, but slightly worse than NC group.

Low TV value indicates insufficient lung ventilation, while high TV value indicates excessive ventilation. MV value is related to TV and respiratory rate. With a small TV value, a higher respiratory rate is needed to ensure adequate ventilation. Pulmonary diseases such as IPF are often characterized by shallow and fast breathing, decreased TV value and increased respiratory rate. The decrease of TV value and MV value can be used as early diagnostic indicators of IPF. As shown in Fig. 5A, TV value of rats in bleo group decreased, which was significantly different from that in NC group ($P < 0.01$). Compared with bleo group, bleo+nidanib group was significantly higher ($P < 0.01$), with a very significant difference ($P < 0.01$), and bleo+Sal B-DPI group also increased, with significant difference ($P < 0.05$). While bleo+Sal B iv group also increased, but there was no significant difference. The MV of bleo group was significantly lower than that of NC group($P < 0.01$). Compared with bleo group, bleo+nidanib group and bleo+Sal B-DPI group were significantly higher ($P < 0.01$), and bleo+Sal B iv group were significantly higher ($P < 0.05$).

As shown in Fig. 5B, the lung tissue structure of NC group rats is clear and intact, with thin alveolar walls, no bleeding points, and normal morphological structure. There was no infiltration and exudation of inflammatory cells and less collagen deposition in the alveolar cavity. Bleo group showed alveolar wall congestion, inflammatory cell infiltration and emphysema. After nidanib, Sal B-DPI and intravenous injection of Sal B solution, the degree of alveolar wall congestion, inflammatory cell infiltration and emphysema in the lung tissue of rats were lower than that of bleo group, bleo+Sal B-DPI group and bleo+nidanib group had better therapeutic effects.

IPF is a common alveolar disease in which healthy lung tissue is replaced by excessive interstitial cells and extracellular matrix, resulting in the destruction of alveolar structures and the gradual densification of alveolar areas, eventually leading to respiratory failure and even death [1–6]. At present, studies have shown that IPF was associated with stages of oxidative stress, inflammatory response and

fibrosis [2–5]. Oxidative stress caused by oxidation/antioxidant imbalance is one of the important factors in the pathogenesis of IPF, and MDA content can reflect the degree of lipid peroxidation in the body. MPO is mainly secreted and catalyzed by neutrophils to produce excessive oxidizing substances, leading to oxidative stress and oxidative tissue damage. SOD can scavenge oxygen free radicals and prevent cells from being damaged by free radicals. TGF-β1 is an important pro-fibrosis factor, which can inhibit its expression, thereby inhibiting the proliferation and activation of fibroblasts, inhibiting collagen synthesis, and reducing extracellular matrix deposition. In the process of pulmonary fibrosis, the increased expression of a variety of inflammatory factors will also cause inflammation and fibrosis. The imbalance of Th1/Th2 in the BALF plays an important role in the pathogenesis of pulmonary fibrosis, and various cytokines secreted by Th1 cells and Th2 cells are involved in the formation of pulmonary fibrosis. Th2 cytokines, such as IL-1β, IL-4, IL-6 and IL-18, can all cause alveolar inflammation and damage in the early stage of pulmonary fibrosis, leading to the activation and proliferation of fibroblast cells and collagen synthesis, leading to matrix protein deposition and production of fibrous tissue [53]. IFN-γ is a Th1 cytokine that inhibits the proliferation of fibroblasts and the formation of fibrous tissue [54]. Hyp is one of the twelve nonessential amino acids that is characteristic of collagen and is a major component of the extracellular matrix during the development of fibrosis in various organs [55].

The MDA content in the lung tissue homogenate of rats in the bleo group was significantly higher than that in NC group($P < 0.01$), and the serum MPO content was also significantly higher than that in NC group($P < 0.01$). The content of MDA and MPO in bleo+nidanib group , bleo+Sal B-DPI group, and bleo+Sal B iv group can be significantly reduced. Bleo+Sal B-DPI group and bleo+nidanib group had a more significant reduction in MDA and MPO content. Compared with NC group, the SOD activity in the lung tissue homogenate of the bleo group was significantly reduced ($P < 0.01$). The SOD activity of bleo+nidanib group, bleo+Sal B-DPI group, and bleo+Sal B iv group increased significantly, but the improvement effect was more significant in bleo+Sal B-DPI group and bleo+nidanib group, as shown in Fig. 5C.

Compared with NC group, the contents of TGF-β1 protein, IL-1β, IL-4, IL-6 and IL-18 in bleo group were significantly increased ($P < 0.01$), and the contents of IFN-γ were significantly decreased ($P < 0.01$). Compared with bleo group, the contents of TGF-β1 protein, IL-1β, IL-4, IL-6 and IL-18 were significantly decreased in bleo+nidanib group and bleo+Sal B-DPI group, and the contents of IFN-γ were significantly increased($P < 0.01$). TGF-β1 protein, IL-6 ($P < 0.01$) and IL-1β, and IL-18 ($P < 0.05$) were significantly decreased in bleo+Sal B iv group, but IL-4 and IFN-γ contents were not significantly different from those in the bleo group, as shown in Fig. 5D.

Compared with NC group, the content of Hyp in lung tissue homogenate of bleo group was significantly increased ($P < 0.01$). Compared with bleo group, the levels of Hyp were significantly lower in bleo+nidanib group, bleo+Sal B-DPI group and bleo+Sal B iv group. However, bleo+Sal B-DPI group and bleo+nidanib group had a more significant reduction effect ($P < 0.01$), as shown in Fig. 5E.
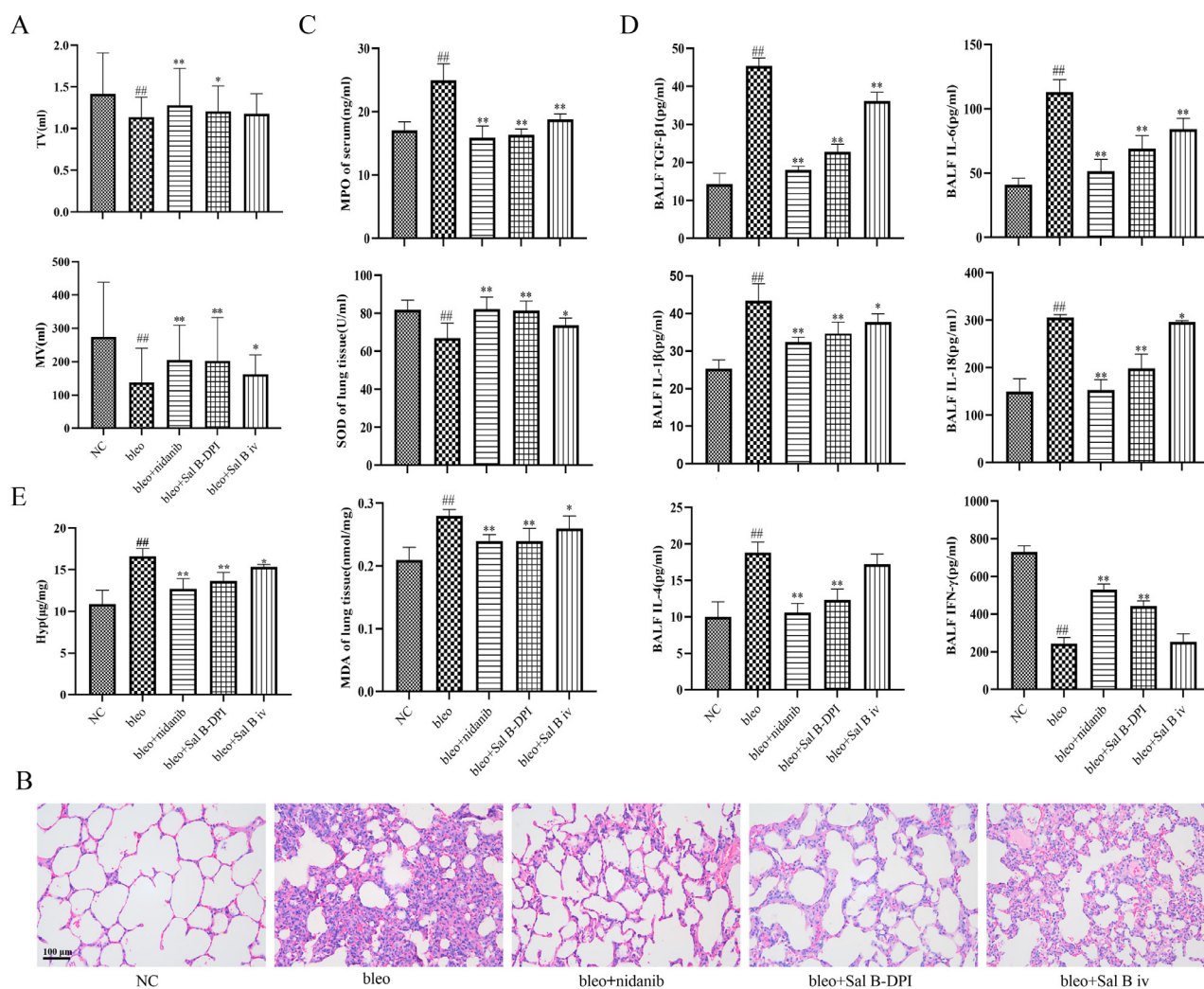
Fig. 5 – Preliminary pharmacodynamics study *in vivo*. (A) Pulmonary function indexes of rats (Mean±SD, *n* = 6).(B) Hematoxylin&eosin (H&E) staining of rat lung tissue (×200). (C) Comparison of MPO contents in serum, SOD and MDA contents in lung homogenate (Mean ± SD, *n* = 6). (D) The concentrations of inflammatory factors and IFN-*γ* in BALF(Mean ± SD, *n* = 6).(E) Comparison of Hyp content in lung tissue(Mean ± SD, *n* = 6). ## *P* < 0.01 vs NC group, *P < 0.05, ** *P* <0.01 vs bleo group.

3.6. Metabonomics study of lung tissue in rats

Multivariate statistical analysis is mostly used to deal with the characteristics of complex sample classification by dimensionality reduction. Its core idea is to condense multiple variables into one or two with the strongest characteristics through variance changes. As shown in Fig. S3, A1 showed the scatter diagram of PCA analysis of multiple groups. Each sample in each group presents a certain natural aggregation state under the projection of principal component analysis, and this characteristic is further strengthened in OPLS-DA analysis (Fig. S3A2). This indicates that there are certain similarities among each sample group, that is, common characteristics, and there are significant differences among each group.

To further search for and characterize the difference components, OPLS-DA between the two groups was used to screen potential metabolic markers, as shown in Fig. 12B-

12E. The R^2Y and Q^2 parameters of OPLS-DA were all close to 1. The replacement test analysis showed that the model established by OPLS-DA in each group was good without over-fitting (Table S2), which could be used for further screening of candidate metabolic markers based on VIP value. In the multivariate statistical analysis of the negative ion mode, compared with the model group, the Q^2 parameter of OPLS-DA in the pulmonary administration of Sal B-DPI group (F) and intravenous injection of Sal B solution group (W) was less than 0.9 but greater than 0.5, which was still an effective model and could be further analyzed. The specific results were shown in Fig. S4 and Table S3.

In the OPLS-DA discriminant model based on multivariate statistical analysis, VIP parameters were used as the Cut off for screening differential endogenous small molecules through supervision and identification. On the basis of VIP > 1, Metlin and HMDB online databases were used to identify the sources (endogenous, exogenous, drug-derived, etc.) and

the distribution of body fluids (serum, urine, bile, tissue, etc.) of each feature, screen the endogenous ion peak of lung tissue, and confirm the final difference components by MS/MS and PPM. The HMDB database was used to compare the primary excimer ion peaks of the differential components according to the precise molecular weight, and the final differential components were confirmed by MS/MS and ppm. $T = 5.88$ min, m/z 496.3406) was used as an example to illustrate the identification process of the compounds. Firstly, m/z 496.3406 was used to conduct an accurate molecular weight search in the HMDB database, ppm was set to 15, and the ion summation forms were $M + H$, $M+Na$, $M+NH_4$, $M + K$, $M+Li$, etc., for matching. Then, on the basis of matching results, exogenous components were eliminated and only endogenous components were retained. The molecular composition was preliminarily determined to be $C_{24}H_{50}NO_7P$, ppm $=1.61<<15$. Then, based on MassLYNX and QI workstations, the precise molecular weight of the component was searched, and its MS/MS at RT=5.87 was obtained. As shown in Fig. S5, the mass spectrum fragments of m/z 104.1078, 125.0009 and 184.0743 correspond to $-C_5H_{13}NO$, $-C_9H_{17}$, $-C_5H_{13}NO_4P$, and basically determine that m/z 496.3406 and RT=5.87 were LYSOPC (16:0/0:0) .

As shown in Fig. S6, a total of 23 differential endogenous metabolites were identified based on UPLC-Q-TOF/MS in the positive and negative ion mode. After administering the positive drug nintedanib to rats, the 23 disease markers can be recalled to 7 [3-Methyl-2-butene-1-thiol, Indole-3-carboxaldehyde, LysoPC (P-18:0/0:0)), SM (d18:1/16:1), Indoleacrylic acid, L-Cystine and Hypoxanthine] ($P<0.05$); after pulmonary administration of Sal B-DPI to rats, 23 disease markers can be recalled 7 [LysoPC (14:0/0:0), LysoPC (P-18:0/0:0), PE (16:0/15:0), PC (18:4/18:1), SM (d18:1/16:1), L-Cystine and Hypoxanthine] ($P <0.05$); after administration of Sal B solution to rats via the tail vein route, 23 disease markers can be recalled 3 [PE(16:0/15 :0), PC (22:6/18:2) and L-Cystine] ($P <0.05$). Bleo+Sal B-DPI group is equivalent to bleo+nintedanib group. In addition, through metabolic pathway analysis, it was found that the differential metabolites in bleo+Sal B-DPI group were mainly enriched in four pathways: glycerophospholipid metabolism, linolenic acid metabolism, α-linolenic acid metabolism and glycosylphosphatidylinositol anchor biosynthesis(Fig. S7).

3.7. Preliminary pharmacokinetics and lung tissue distribution study

Duration curves of Sal B at different times after pulmonary administration of Sal B-DPI(Sal B-DPI group) and intravenous injection of Sal B solution(Sal B iv group) were shown in Fig. S8A. According to the blood concentration of Sal B, WinNonlin 6.4 software was used to calculate the pharmacokinetic parameters, as shown in Table 3. T_{max} of Sal B-DPI group and Sal B iv were 0.083 and 0.033 h, respectively. The C_{max} values were 8012.26±751.84 and 16,404.17±2237.56 ng/ml, respectively, and the differences were extremely significant ($P < 0.01$). AUC$_{0-\infty}$ was 3841.29±515.73 and 6554.95±1485.24 h•ng/ml, respectively, with extremely significant difference ($P < 0.01$). The absolute bioavailability of Sal B was 59.67%±6.30% for Sal B -DPI group.

Table 3 – Pharmacokinetic parameters of Sal B in rats plasma after intravenous injection of Sal B solution and pulmonary administration of Sal B-DPI(Mean ± SD, $n = 6$).

Parameters	Units	Sal B iv	Sal B-DPI
C_{max}	ng/ml	16,404.17±2237.56	8012.26±751.84**
T_{max}	h	0.033±0.00	0.083±0.00
AUC$_{0-\infty}$	h•ng/ml	6554.95±1485.24	3841.29±515.73**
Lz	1/h	0.45±0.07	0.28±0.11**
$T_{1/2}$	h	1.56±0.28	2.72±0.93*
Vz/F	l/kg	5.62±1.47	13.20±4.12**
Cl/F	l/ h/kg	2.49±0.47	3.39±0.33**
MRT	h	0.83±0.10	0.58±0.10**

AUC, area under the concentration–time curve; Cl/F, clearance; C_{max}, maximum concentration; Lz, elimination of phase slope; MRT, mean residence time; $T_{1/2}$, distribution half-life; T_{max}, time to reach maximum concentration; Vz/F, aparent volume of distribution.
* $P < 0.05$,.
** $P < 0.01$, compared with Sal B iv group.

Table 4 – Pharmacokinetic parameters of Sal B in rat lung tissue after intravenous injection of Sal B solution and pulmonary administration of Sal B-DPI (Mean±SD, $n = 3$).

Parameters	Units	Sal B iv	Sal B-DPI
C_{max}	ng/g	13,150.38±619.02	142,594.47±3654.22**
T_{max}	h	0.033±0.00	0.033±0.00
AUC$_{0-\infty}$	h•ng/g	1898.5 ± 134.03	80,583.35±4225.84**
Lz	1/h	0.77±0.04	0.62±0.04**
$T_{1/2}$	h	0.9 ± 0.05	1.12±0.07*
Vz/F	g/kg	7517.28±902.65	285.35±17.27**
Cl/F	g/h/kg	5778.96±452.59	176.26±6.39**
MRT	h	0.19±0.00	0.72±0.03**

* $P < 0.05$,.
** $P < 0.01$ vs Sal B iv group.

The distribution of Sal B in the lung tissue after pulmonary administration of Sal B-DPI(Sal B-DPI group) and intravenous injection of Sal B solution(Sal B iv group) were shown in Figure S8B. According to the concentration of Sal B in the lung tissue, WinNonlin 6.4 software was used to calculate the pharmacokinetic parameters in Table 4. T_{max} of Sal B-DPI group and Sal B iv group were 0.033 and 0.033 h, respectively. C_{max} values were 142,594.47±3654.22 and 13,150.38±619.02 ng/ml, respectively, with extremely significant differences ($P < 0.01$). AUC$_{0-\infty}$ was 80,583.35 ± 4225.84 and 1898.5 ± 134.03 h•ng/ml, respectively. AUC$_{0-\infty}$ of Sal B-DPI group was 42.45 times that of Sal B iv group , with significant difference ($P <0.01$).

Some studies reported that the oral bioavailability of Sal B was no more than 5.56% [18–20]. In previous studies, the absolute bioavailability of Sal B was 19.15%±7.44% [41], while the absolute bioavailability of Sal B was 59.67%±6.30% after pulmonary administration of Sal B-DPI. Compared with the oral bioavailability reported in the study, the oral bioavailability increased by nearly 11 times, and the oral bioavailability increased by more than 3 times compared with the previous experimental results, which should be attributed to the reduction of Sal B-DPI particle size and

the improvement of *in vitro* deposition efficiency. From the perspective of systemic absorption, the development of Sal B pulmonary drug delivery system is very promising. The therapeutic effect of drugs is usually directly related to the drug concentration of the target. The concentration of Sal B in lung tissue was still 2940.62±117.04 ng/g after 1 h of pulmonary administration, indicating that dry powder inhalers have certain advantages in the treatment of pulmonary diseases (such as IPF).

4.   Conclusions

In this study, L-leucine as excipient was used to prepare Sal B-DPI successfully by spray drying method, which improved the powder properties, drug delivery efficiency, *in vitro* deposition effect of Sal B-DPI, and enhanced its moisture resistance. In the form of DPI, it was targeted to the lungs through tracheal non-invasive lung drug delivery technology, which had no irritation to the lungs, overcomed the shortcomings of poor oral absorption and low bioavailability of Sal B, increased the drug concentration in the lesion site, and improved the therapeutic effect of IPF. The above work provided new ideas and methods for the clinical treatment of IPF and the clinical application of Sal B.

Conflicts of interest

The authors have no conflicts of interest to declare.

Acknowledgements

Supplementary materials

Supplementary material associated with this article can be found, in the online version, at doi:10.1016/j.ajps.2022.04.004.

REFERENCES

[1] Glass DS, Grossfeld D, Renna HA, Agarwala P, Spiegler P, Kasselman LJ, Glass AD, et al. Idiopathic pulmonary fibrosis: molecular mechanisms and potential treatment approaches. Respir Investig 2020;58:320–35.

[2] Behr J, Günther A, Bonella F, Geißler K, Koschel D, Kreuter M, Prasse A, et al. German guideline for idiopathic pulmonary fibrosis-update on pharmacological therapies 2017. Pneumologie 2018;72:155–68.

[3] Nam JK, Kim AR, Choi SH, Kim JH, Han SC, Park S, et al. Pharmacologic inhibition of HIF-1 alpha attenuates radiation-induced pulmonary fibrosis in a preclinical image

[4] Milara J, Hernandez G, Ballester B, Morell A, Roger I, Montero P, et al. The JAK2 pathway is activated in idiopathic pulmonary fibrosis. Respir Res 2018;19:24.

[5] Wolters PJ, Blackwell TS, Eickelberg O, Loyd JE, Kaminski N, Jenkins G, et al. Time for a change: is idiopathic pulmonary fibrosis still idiopathic and only fibrotic? Lancet Respir Med 2018;6:154–60.

[6] Wu H, Yu Y, Huang H, Hu Y, Fu S, Wang Z, et al. Progressive pulmonary fibrosis is caused by elevated mechanical tension on alveolar stem cells. Cell 2020;180:107–21.

[7] George PM, Wells AU, Jenkins RG. Pulmonary fibrosis and COVID-19: the potential role for antifibrotic therapy. Lancet Respir Med 2020;8:807–15.

[8] Ma L, Wang R, Miao M. Analysis of the law of traditional Chinese medicine for the treatment of pulmonary fibrosis based on data mining. Chin Herbal Med 2020;51: 1406–1411.

[9] Liu Q, Wang R, Qu G, Wang Y, Liu P, Zhu Y, et al. General observation report of systemic anatomy of New Coronavirus Pneumonia deaths. J Forensic Med 2020;36:19–21.

[10] Raghu G, Rochwerg B, Zhang Y, Garcia CA, Azuma A, Behr J, et al. An official ATS/ERS/JRS/ALAT clinical practice guideline: treatment of idiopathic pulmonary fibrosis: an update of the 2011 clinical practice guideline. Am J Respir Crit Care Med 2015;192:e3.

[11] Mulhall A, Cole A, Patel S. Efficacy and safety of nintedanib in idiopathic pulmonary fibrosis, cytisine *versus* nicotine for smoking cessation, and FACED score for non-cystic fibrosis bronchiectasis. Am J Respir Crit Care Med 2015;192:249–51.

[12] King TE, Bradford WZ, Castro-Bernardini S, Fagan EA, Glaspole I, Glassberg MK, et al. ASCEND study group. A phase 3 trial of pirfenidone in patients with idiopathic pulmonary fibrosis. N Engl J Med 2014;370:2083–92.

[13] Li LC, Kan LD. Traditional chinese medicine for pulmonary fibrosis therapy: progress and future prospects. J Ethnopharmacol 2017;198:45–63.

[14] Zhang YK, Lu P, Qin H, Zhang Y, Sun X, Song X, et al. Traditional Chinese medicine combined with pulmonary drug delivery system and idiopathic pulmonary fibrosis: rationale and therapeutic potential. Biomed Pharmacother 2021;133:111072.

[15] Nwafor EO, Lu P, Li J, Zhang Q, Qi D, Liu Z, et al. Traditional chinese medicine of Salvia miltiorrhiza Bunge: a review of phytochemistry, pharmacology and pharmacokinetics. Tradit Med Res 2021;6:35.

[16] Jiang L, Wang J, Ju J, Dai J. Salvianolic acid B and sodium tanshinone II A sulfonate prevent pulmonary fibrosis through anti-inflammatory and anti-fibrotic process. Eur J Pharmacol 2020;883:173352.

[17] Liu Q, Shi X, Tang L, Xu W, Jiang S, Ding W, et al. Salvianolic acid B attenuates experimental pulmonary inflammation by protecting endothelial cells against oxidative stress injury. Eur J Pharmacol 2018;840:9–19.

[18] Zhou L, Chow MSS, Zuo Z. Effect of sodium caprate on the oral absorptions of danshensu and salvianolic acid B. Int J Pharm 2009;379:109–18.

[19] Gao DY, Han LM, Zhang LH, Fang XL, Wang JX. Bioavailability of salvianolic acid B and effect on blood viscosities after oral administration of salvianolic acids in beagle dogs. Arch Pharm Res 2009;32:773–9.

[20] Wu YT, Chen YF, Hsieh YJ, Jaw I, Shiao MS, Tsai TH. Bioavailability of salvianolic acid B in conscious and freely moving rats. Int J Pharm 2006;326:25–31.

[21] Orienti I, Gentilomi GA, Farruggia G. Pulmonary delivery of fenretinide: a possible adjuvant treatment in COVID-1. Int J Mol Sci 2020;21:3812.

guided radiation therapy. Int J Radiat Oncol Biol Phys 2021;109:553–66.

[22] Chandel A, Goyal AK, Ghosh G, Rath G. Recent advances in aerosolised drug delivery. Biomed Pharmacother 2019;112:108601.

[23] Mönckedieck M, Kamplade J, Fakner P. Spray drying of mannitol carrier particles with defined morphology and flow characteristics for dry powder inhalation. Dry Technol 2017;35:1843–57.

[24] de Boer AH, Hagedoorn P, Hoppentocht M, Buttini F, Grasmeijer F, Frijlink HW. Dry powder inhalation: past, present and future. Expert Opin Drug Deliv 2017;14:499–512.

[25] Weers JG, Miller DP, Tarara TE. Spray-dried pulmosphere™ formulations for inhalation comprising crystalline drug particles. AAPS PharmSciTech 2019;20:103.

[26] Shetty N, Park H, Zemlyanov D, Mangal S, Bhujbal S, Zhou QT. Influence of excipients on physical and aerosolization stability of spray dried high-dose powder formulations for inhalation. Int J Pharm 2018;544:222–34.

[27] Li L, Sun S, Parumasivam T, Denman JA, Gengenbach T, Tang P, et al. L-Leucine as an excipient against moisture on in vitro aerosolization performances of highly hygroscopic spray-dried powders. Eur J Pharm Biopharm 2016;102:132–41.

[28] Eedara BB, Rangnekar B, Doyle C, Cavallaro A, Das SC. The influence of surface active L-leucine and 1,2-dipalmitoyl-sn-glycero-3-phosphatidylcholine (DPPC) in the improvement of aerosolization of pyrazinamide and moxifloxacin co-spray dried powders. Int J Pharm 2018;542:72–81.

[29] Kyriakoudi A, Tsimidou MZ. Properties of encapsulated saffron extracts in maltodextrin using the Büchi B-90 nano spray-dryer. Food Chem 2018;266:458–65.

[30] Boer AH, Gjaltema D, Hagedoorn P, Schaller M, Witt W, Frijlink HW. Design and application of a new modular adapter for laser diffraction characterization of inhalation aerosols. Int J Pharm 2002;249:233–45.

[31] Pilcer G, Wauthoz N, Amighi K. Lactose characteristics and the generation of the aerosol. Adv Drug Deliv Rev 2012;64:233–56.

[32] Mohamed JMM, Alqahtani A, Al Fatease A, Alqahtani T, Khan BA, Ashmitha B, et al. Human hair keratin composite scaffold: characterisation and biocompatibility study on NIH 3T3 fibroblast cells. Pharmaceuticals (Basel) 2021;14(8):781.

[33] Awaluddin R, Nugrahaningsih DAA, Solikhah EN. The concentration -dependent pro-fibrotic effect of metformin on LPS and high glucose induced fibroblast NIH 3T3 and Macrophage RAW 264.7 Cell co-culture. Med J Malaysia 2020;75(1):10–13 Suppl.

[34] Sergi R, Bellucci D, Salvatori R, Cannillo V. Chitosan-based bioactive glass gauze: microstructural properties, in vitro bioactivity, and biological tests. Materials (Basel) 2020;13(12):2819.

[35] Lelli D, Sahebkar A, Johnston TP, Pedone C. Curcumin use in pulmonary diseases: state of the art and future perspectives. Pharmacol Res 2017;115:133–48.

[36] Labiris NR, Dolovich MB. Pulmonary drug delivery. Part I: physiological factors affecting therapeutic effectiveness of aerosolized medications. Br J Clin Pharmacol 2015;56:588–99.

[37] Lv Z, Huang K, Gan W, Gao S, Yang B, Helian K, et al. Comparison of the efficacy of pirfenidone and nintedanib in inhibiting bleomycin-induced pulmonary fibrosis in mice. Chin J Pathophysiol 2020;36:112–18.

[38] Liu C, Gu C, Huang W, Sheng X, Du J, Li Y. Targeted UPLC-MS/MS high-throughput metabolomics approach to assess the purine and pyrimidine metabolism. J Chromatogr B Analyt Technol Biomed Life Sci 2019;1113:98–106.

[39] Lu P, Xing Y, Xue Z, Ma Z, Zhang B, Peng H, et al. Pharmacokinetics of salvianolic acid B, rosmarinic acid and Danshensu in rat after pulmonary administration of Salvia miltiorrhiza polyphenolic acid solution. Biomed Chromatogr 2019;33:e4561.

[40] National Pharmacopoeia Commission Pharmacopoeia of the people's republic of china. Beijing: China Medical Science and Technology Press; 2020.

[41] Lu P, Xing Y, Peng H, Liu Z, Zhou QT, Xue Z, et al. Physicochemical and pharmacokinetic evaluation of spray-dried coformulation of salvia miltiorrhiza polyphenolic acid and L-leucine with improved bioavailability. J Aerosol Med Pulm Drug Deliv 2020;33:73–82.

[42] Boraey MA, Hoe S, Sharif H. Improvement of the dispersibility of spraydried budesonide powders using leucine in an ethanol-water cosolvent system. Powder Technol 2013;2362:171–8.

[43] Jiang L, Li Y, Yu J, Wang J, Ju J, Dai J. A dry powder inhalable formulation of salvianolic acids for the treatment of pulmonary fibrosis: safety, lung deposition, and pharmacokinetic study. Drug Deliv Transl Res 2020.

[44] Yang J, Han L, Shao R, Zhang P, Hao J, Chang Y, et al. Study on the effect of chinese patent medicine on inhibiting fibroblast collagen deposition. Tianjin J Tradit Chin Med 2020;37:618–22.

[45] Zhang L, Wang Y, Wu G, Xiong W, Gu W, Wang CY. Macrophages: friend or foe in idiopathic pulmonary fibrosis? Respir Res 2018;19:170.

[46] Beigi Harchegani A, Tahmasbpour E, Borna H, Imamy A, Ghanei M, Shahriary A. Free radical production and oxidative stress in lung tissue of patients exposed to sulfur mustard: an overview of cellular and molecular mechanisms. Chem Res Toxicol 2018;31:211–22.

[47] Dorhoi A, Kaufmann SH. Pathology and immune reactivity: understanding multidimensionality in pulmonary tuberculosis. Seminars in Immunopathol 2016;38:153–66.

[48] Bueno M, Calyeca J, Rojas M, Mora AL. Mitochondria dysfunction and metabolic reprogramming as drivers of idiopathic pulmonary fibrosis. Redox Biol 2020;33:101509.

[49] Snijder J, Peraza J, Padilla M, Capaccione K, Salvatore MM. Pulmonary fibrosis: a disease of alveolar collapse and collagen deposition. Expert Rev Respir Med 2019;13:615–19.

[50] Mierzejewski M, Korczynski P, Krenke R, Janssen JP. Chemical pleurodesis-a review of mechanisms involved in pleural space obliteration. Respir Res 2019;20:247.

[51] Gautret P, Million M, Jarrot PA, Camoin-Jau L, Colson P, Fenollar F, et al. Natural history of COVID-19 and therapeutic options. Expert Rev Clin Immunol 2020;16:1159–84.

[52] Kolb P, Upagupta C, Vierhout M, Ayaub E, Bellaye PS, Gauldie J, et al. The importance of interventional timing in the bleomycin model of pulmonary fibrosis. Eur Respir J 2020;55:1901105.

[53] Kang MJ, Yoon CM, Nam M, Kim DH, Choi JM, Lee CG, et al. Role of chitinase 3-Like-1 in interleukin-18-induced pulmonary type 1, type 2, and type 17 inflammation; alveolar destruction; and airway fibrosis in the murine lung. Am J Respir Cell Mol Biol 2015;53:863–71.

[54] Smaldone GC. Repurposing of gamma interferon via inhalation delivery. Adv Drug Deliv Rev 2018;133:87–92.

[55] Wu Z, Hou Y, Dai Z, Hu CA, Wu G. Metabolism, nutrition, and redox signaling of hydroxyproline. Antioxid Redox Signal 2019;30:674–82.